The main S&T results in the project.

The overall goal with this project has been to develop nanowire structures for LED applications, notably for visible light emission, i.e. so called Solid State Lighting (SSL). This involves research on suitable growth procedures for the complex LED configurations involved. The nanowire topology means that the characterization of the relevant physical properties partly requires novel experimental techniques, adapted to the nanowire geometry. A complete characterization would ideally involve sub-nm resolution of the measured properties, not yet realistic. To verify that the results in growth and characterization lead to the projected properties of the nano-wire based LEDs (NW-LEDs), a pilot production facility has been established at one of the industry partners (GLOINC). The results obtained from the evaluation of the produced NW-LEDs form a relevant basis for the evaluation of the progress as well as remaining problems in the application of NW-LEDs for SSL purposes.

The most important details of the results obtained will be described in what follows, following the structure of the different work packages. In the growth area it is clear that the MOCVD technique has proven to be a useful vehicle to produce complex core-shell NW-LED structures with nm precision. This does not mean that problems are not present. It is clear that the obtained irregular results of the efficiency of blue NW-LED emitters involve a defect problem that is not directly revealed by the experimental investigations. Likewise the rather strong droop observed for green emitters is not expected from the presently accepted theory, it may be viewed as another evidence for nm size structural defects related to the complex geometry of these NWs. More research is obviously needed before such problems are under control.

In the characterization work package important developments have taken place in optical methods, electron microscopy and XRD techniques. The electron holography techniques can now be used with confidence since the influence of electron irradiation on defect creation during the experiments has been understood. The potential profile across a single NW-LED structure can now be mapped out, which is very valuable to understand other data, such as electrical measurements. Photoluminescence (PL) and cathodoluminescence (CL, both at temperatures down to 5 K) are valuable to understand the nature of the radiative transitions in the LEDs, the latter technique also has the spatial resolution to study variations of emission across a single NW-LED. A suitable platform for electrical measurements on single NW-LEDs has been developed and used in the project.

The third work package is focused on demonstrating a device processing technology for the studied NW-LEDs, by using a wafer process flow running on a commercial wafer fabrication line. One important task is to compare the predicted performance of the NW-LEDs with reality, in terms of lumen and color maintenance, wall-plug efficiency, reliability, and predicted production cost. GLOINC has demonstrated that it is possible to produce nanowire LEDs using a flip-chip process technology, thereby enabling the integration of these LEDs into systems with large numbers of devices. The reliability tests also show that these devices

behave very similarly to the commercial planar LEDs. As mentioned above there are still some areas where more work is needed to understand the behavior, e.g, the lower average emission intensity from the blue NW-LEDs (as compared to the planar violet-blue LEDs) and the excessive droop of the green NW-LEDs.

Below some important results in the project will be described in more detail.

WP1. MOCVD growth technology for III-nitride and III-V NW-LED structures.

The III-N NW LED structure consists typically of a Si-doped GaN core in the shape of a pillar grown perpendicular to the wafer surface. The GaN core is of wurtzite crystal structure and acts as a template for a radially grown InGaN quantum well acting as an active region for the LED device, an electron blocking AlGaN shell and a Mg-doped GaN: p-GaN shell as a source of holes injected to the active layer, where they can recombine with electrons and generate light. The vertical form of nanowire is beneficial for enhancing light extraction. A schematic representation of the NW LED cross-section along a cut perpendicular to the *m*-plane can be seen in Fig. 1a. A complementary cross-section view from SEM on a typical NW LED is shown in Fig. 1b.

The growth template consists of a silicon substrate, of (111) orientation, or a c-plane sapphire wafer. An AlGaN/AlN wetting layer is grown before the main buffer layer, which is a 2-4 µm Si-doped thick GaN layer, with Si doping in the range 1-5 E18 cm^{-3}. A silicon nitride mask was deposited on the GaN layer, with a thickness ranging from 30 to 50nm. Electron beam lithography (EBL) or nanoimprint lithography (NIL) have been used to make openings in the silicon nitride mask down to the GaN layer. The typical opening aperture ranges between 70 to 140 nm, however in this project we have also tested openings up to 300 nm. The openings form a honeycomb pattern, with a pitch distance between the nearest neighbors varying between 1 and 1.5 µm. These openings define the positions and dimensions of the grown nanowires. To determine the surface morphology scanning electron microscopy was performed on nanowire samples. A Thermal Field Emission Scanning Electron Microscope (SEM) LEO 1560 was used, with 10 kV electron acceleration voltage. Cathodoluminescence (CL) was performed at Lund University (ULUND), using a Cambridge Instruments S250 M3 SEM, with a GaAs photomultiplier tube (PMT) recording the CL spectra, and with a cooling stage capable of cooling the sample to below 5 K. Photoluminescence (PL) data was recorded using a micro-PL setup at Lund University, with an excitation laser at 375nm, 9mW.

In order to ensure controlled growth of NW LEDs, nanowire cores must be grown uniformly from the mask openings. Since different pitch and different hole size was used, it is important to use proper nucleation conditions. In the initial nucleation step the flows of TEGa as Ga precursor and NH3 as N precursor were optimized for various pitch/hole sizes. Effects of thermal pre-annealing as well as nucleation and nanowire core growth temperature were taken into account. After nucleation, TEGa and NH3 were continuously flown to ensure the targeted nanowire length. The results of nanowire diameter in respect to growth time in the case of EBL 1 µm /70nm openings are shown in Figure 2a, and the dependence of *m*-plane length on growth time are shown in Fig. 2b.

As seen in Fig 2a. the diameter is enlarged in the first 30 seconds of growth, after which it has stabilized at about 160 nm. The *m*-plane length increases linearly with the growth time. Based on the initial growth stage findings and by applying volume growth rate calculations to different pitch/opening size we have obtained uniform growth of NW LEDs on available substrates as shown in Fig.3.

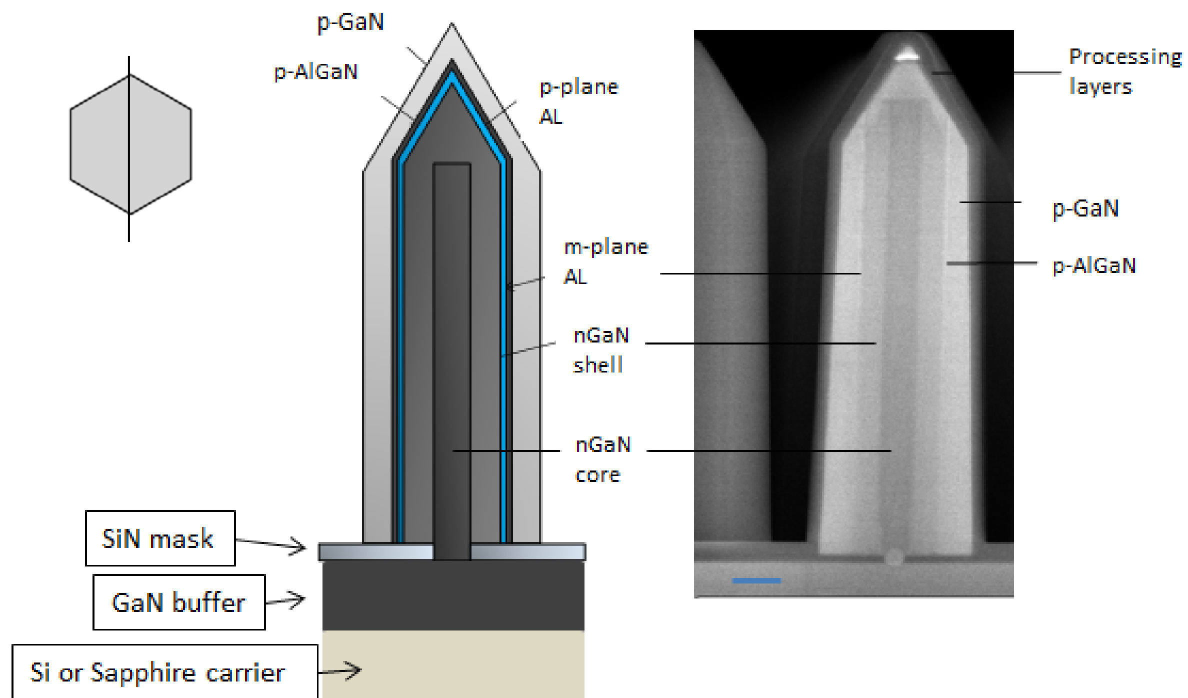

Fig.1. a) to the left. Schematic cross-section of III-N nanowire LED. b) to the right. Cross-sectional SEM image taken at 80k magnification. The scale bar is 200 nm.

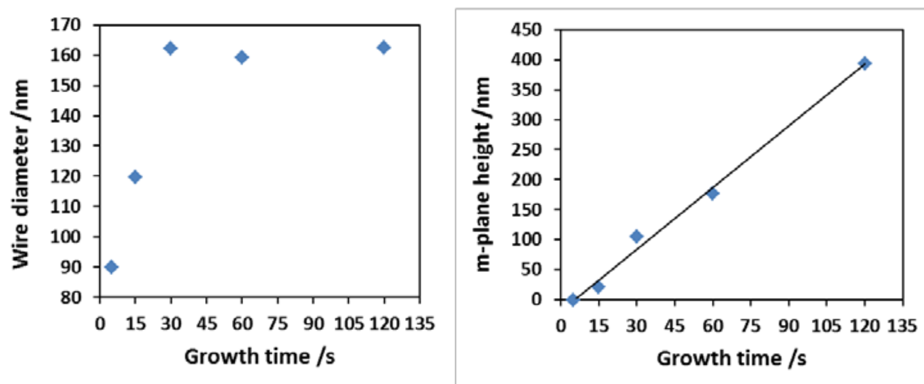

Fig.2. a) dependence of nanowire diameter on growth time in initial growth stages. b) dependence of m-plane length on growth time in the initial growth stages.

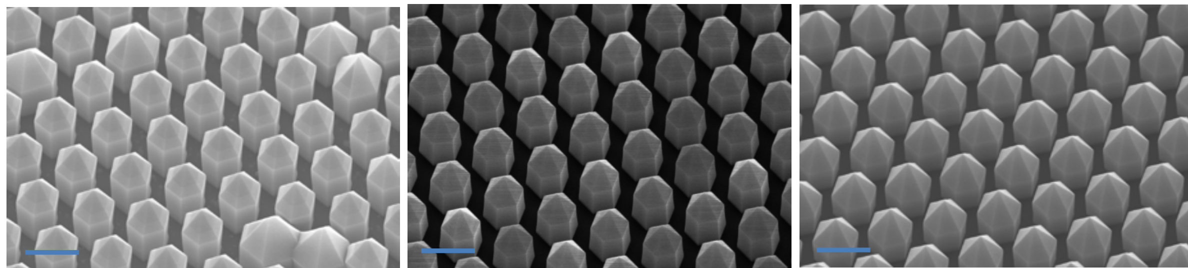

Fig.3. 30 deg tilted SEM picture on NW LEDs on different pitch/opening aperture templates: EBL 1 µm/70nm to the left, NIL 1 µm/100nm in the middle and NIL 1.5µm/140nm to the right. The scale bar is 1 µm.

The typical diameter of the NW core is dependent on the mask-opening aperture and varies between 190-220 nm for a hole size 70 to 100 nm. Nanowires up to 3µm in length could be grown with good growth uniformity. The structural quality of all internal layers in a NW-LED was characterized by transmission electron microscopy (TEM). As seen in cross-sectional TEM in Figure 4 no stacking faults or dislocations are observed in NW core/nGaN shell. This was possible to achieve through careful selection of growth conditions for each individual layer.

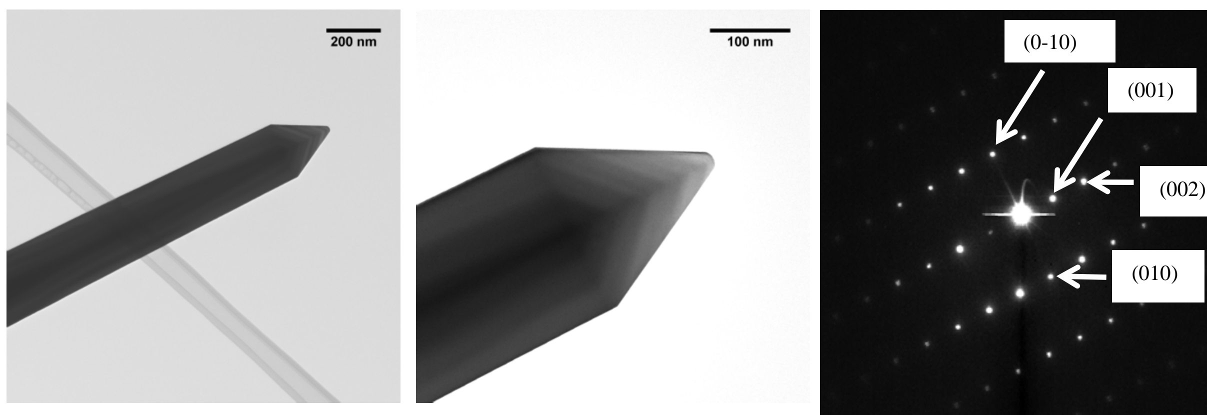

Fig.4. To the left: high resolution TEM on an NW nGaN core - overview. In the centre: magnification on the tip region. To the right: Electron diffraction pattern taken in zone [100], perpendicular to the NW long axis.

The side and pyramid facets were determined by electron diffraction in TEM. As expected the side of the nanowire is terminated by {1-100} facets (non-polar *m*-plane), while tip facets are semi-polar and have {1-101} orientation. The LED structure was extended by outer shells like InGaN QW/p-AlGaN/p-GaN grown on top of the nGaN shell. The outer shells are grown following the {1-100} and {1-101} crystallographic orientations.

Optical and electrical characterization of III-N NW LEDs.

We have grown and characterized InGaN and p-GaN layer shells using proprietary Glo technology. A uniform distribution of indium in the QWs as well as uniform growth of the QWs are important to ensure monochromatic light extraction. Indium segregation as spatial variation in indium composition is one of the issues for the QWs. To determine spatial distribution and variation of indium composition in an SQW as well as Mg dopants in the p-layers, InGaN and p-GaN shells were characterized by cathodoluminescence at a temperature of 4 K. Fig.5 shows spatially resolved CL of an NW SQW LED, taken at 7K. From spatially resolved CL spot mode we were able to determine that there is a shift in QW emission

towards shorter wavelenths when moving the measurement spot from the top of the nanowire towards the bottom. The emission at the EL peak WL from SQW could from about 470nm on the top to about 430 nm at the bottom. This could be due to non-uniform indium incorporation as well as non-uniform QW thickness along the *m*-plane. However, no stacking faults or dislocations in the QWs were observed in TEM.

We postulate that indium incorporation could be improved by a change in growth conditions such as QW temperature and pressure as well as nanowire length, with possible improvement when using shorter nanowires. The CL data was correlated to energy dispersion spectroscopy TEM (EDS TEM), where QW thickness and indium composition have been determined. In Table 1 below EDS and TEM data on indium composition in QW and QW thickness at three spots: bottom, centre and top of the *m*-plane are summarized.

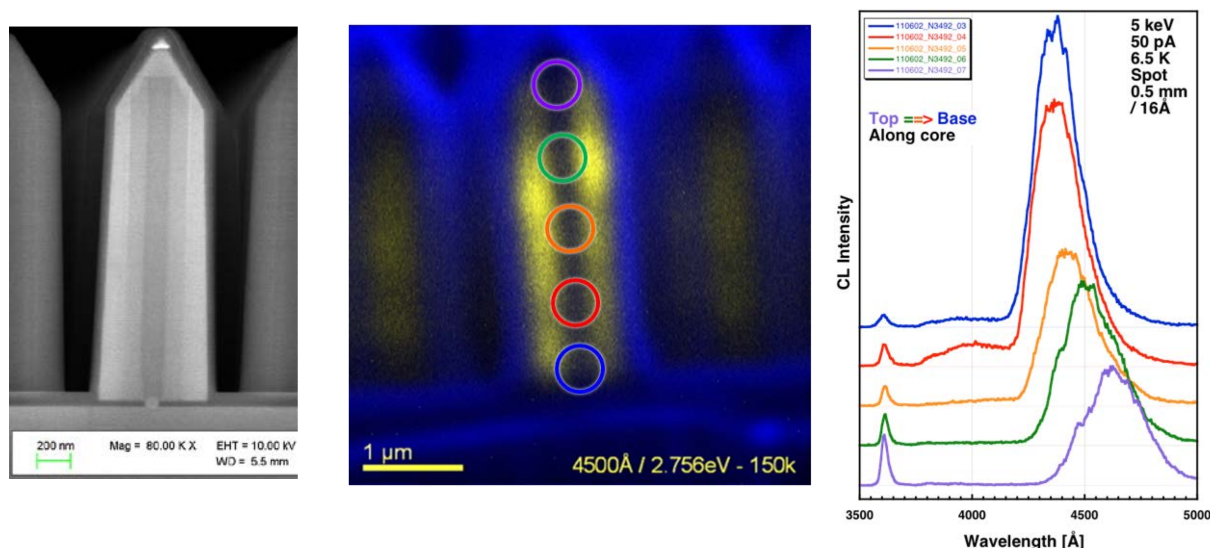

Fig.5. Spatially resolved cathodoluminescence on a single NW LED. Color coded are five spots along the nanowire SQW where CL spectra have been recorded and shown on the plot to the right.

Table. 1. QW thickness by TEM and indium composition by EDS.

	QW top	QW centre	QW bottom
QW thickness (nm)	6.7	5	4.5
In composition (%)	9.3	9.4	6.5

The increase in WL from NW bottom to NW top is consistent with an increase in indium composition and QW thickness from NW base towards NW top. To confirm findings from CL, TEM and EDS we have performed high resolution X-ray diffraction measurements on NW SQWs. As shown in Fig.6. beside several Bragg peaks corresponding to AlGaN wetting layers in the substrate, there is broadening of the (101) peak corresponding to the InGaN

SQW, and this broadening suggests that the QW is fully strained in the out-of-plane direction.

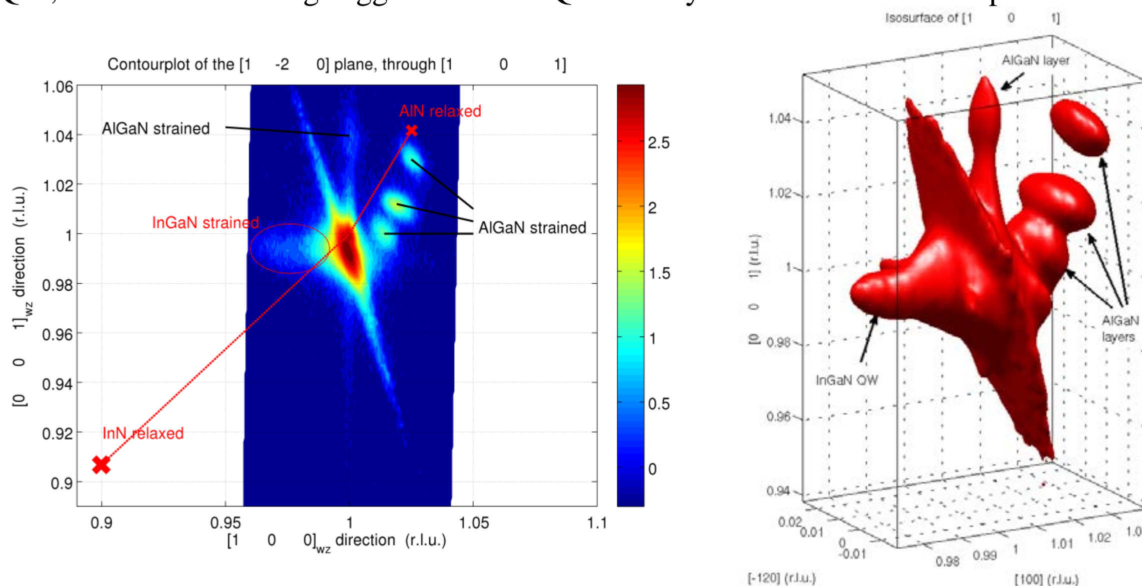

Fig.6. to the left. 3D isosurface of Bragg peaks originating from the wurtzite structure in the InGaN QW. To the right: Contour plot in the (001) direction.

In order to have efficient light generation low resistivity, Mg doped GaN with high hole concentration, at least 5-10 E17 cm^{-3}, must be capping the LED structure. We characterized p-GaN shells either directly on the LED structure or on specially prepared n-p structures consisting only of nGaN core with p-GaN shell. Various characterization techniques have been employed including optical methods such as PL, CL as well as electrical characterization of single n-p nanowire structures. Low temperature PL was performed on p-GaN layers to reveal optical signatures of dopants. Fig.7 shows low temperature (4K) PL spectra taken from ensemble spectra as well as focused micro-PL for single wire spectra.

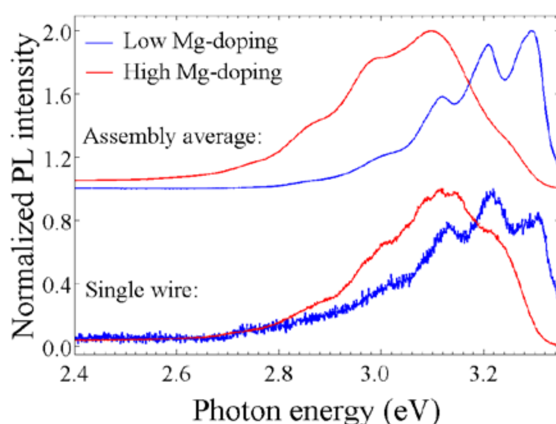

Fig.7. Low temperature photoluminescence on single nanowire pGaN and whole assembly average.

In the near band edge emission (not shown) typical donor bound excitons and acceptor bound excitons are present, The donor-acceptor pair luminescence is dominating the spectra with the peak at 3.27 eV in low Mg doped p-GaN and shifted to 3.0-3.1 eV in high Mg doped p-GaN samples. The PL spectra look similar in case of a measurement on single nanowire as well as from the whole assembly average. The shift in peak position in higher doped pGaN layers has been observed on planar pGaN with atomic Mg incorporation higher than 1E20 cm-3 as determined by SIMS.

Growth of artificially miscut III-N nanowires.

The focus of this work was to realize artificially miscut m-plane sidefacets of GaN nanowires with InGaN single quantum well outer shell. Selective area epitaxy by MOVPE was chosen as a growth technique for this work. Typically the GaN surface on which the InGaN QW is grown is atomically smooth. Indium atoms which exhibit a high surface mobility can easily desorb from the flat GaN surface. A controlled number of nucleation sides like kinks and steps could improve the homogeneity of the grown layer via layer-by-layer growth, and also increase the indium surface incorporation. An increasing indium content in the QW leads to a light emission at longer wavelengths like yellow/red. A controlled layer-by-layer growth mode is desirable to avoid defects, in particular for the growth of the QW active region.

In order to increase the density of steps on GaN surface we have studied the effect of the H2/N2 ratio on n-GaN nanowire tapering, i.e. artificially changing the off-axis angle of m-plane sidefacets. We found out that varying H2/N2 in the gas phase from 0% to 2.78% increases the off-axis angle from about -0.91° (inverse tapered) to 0.6° (tapered nanowire) towards c-plane (growth direction) as shown in Fig.7. However further increase in the H2/N2 ration results in a decrease of this angle. The surface topology was characterized by atomic force microscopy (AFM). Atomic steps on the surface could be distinguished. The mean square roughness increases from 0.3 nm for the baseline with almost 0° miscut angle to 0.75 and 0.6 nm for inverse tapered and tapered nanowire, respectively, thus indicating an increased density of steps with changing artificially the miscut angle.

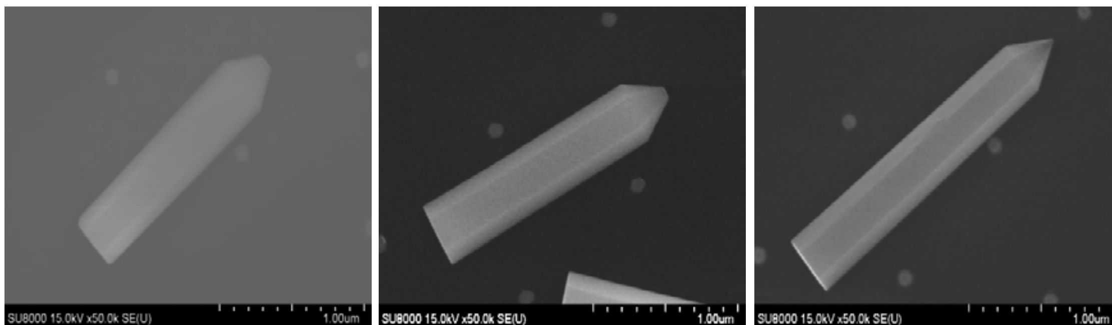

Figure 8. Artificially miscut GaN nanowires. From left to right: miscut angle is 0.91°, 0° and 0.6°.

Blue InGaN QWs aiming for PL emission at about 450nm have been grown on these n-GaN nanowires, and they were characterized by low temperature photoluminescence and cathodoluminescence. Spatially resolved cathodoluminescence presented in Fig. 8 from the inversed tapered nanowire with an off-axis of -0.91° show an EL emission at 500nm at the bottom part of the nanowire, indicating increased indium incorporation at that part. The average EL emission is at 450nm.

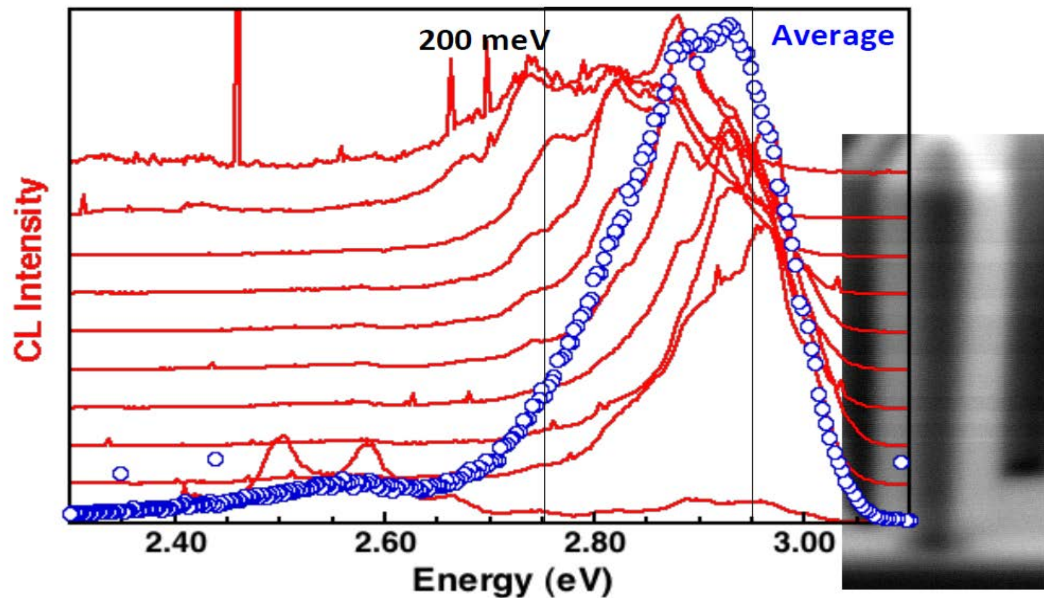

Figure. 9. Spatially resolved CL on inversed tapered nanowire with off-axis angle -0.91°. A series of CL spectra at taken at various positions along the nanowire length.

The above studies are continuing with the aim to optimize the growth conditions of the active QW part of NW-LED structure. We have experienced a large variation in the EQE of the grown violet-blue NW-LEDs, and concluded this is due to a problem with nonradiative defects in the active region of the device, intimately linked to the growth conditions. At the same time there is still an obvious problem with an In-composition gradient along the growth direction.

Growth of dislocation free *c-plane* InGaN platelets based on InGaN nanowires.

A method to fabricate wafer-scale arrays of GaN platelets with a smooth *c-plane* in a submicron size was developed. Such GaN platelets are free of dislocations since they are grown based on InGaN nanowires where the dislocation propagation from the underlying GaN buffer layer can be inhibited. On the *c-plane* of the platelets, high quality nitride layers such as AlGaN and InGaN can be grown for electronic and optoelectronic devices.

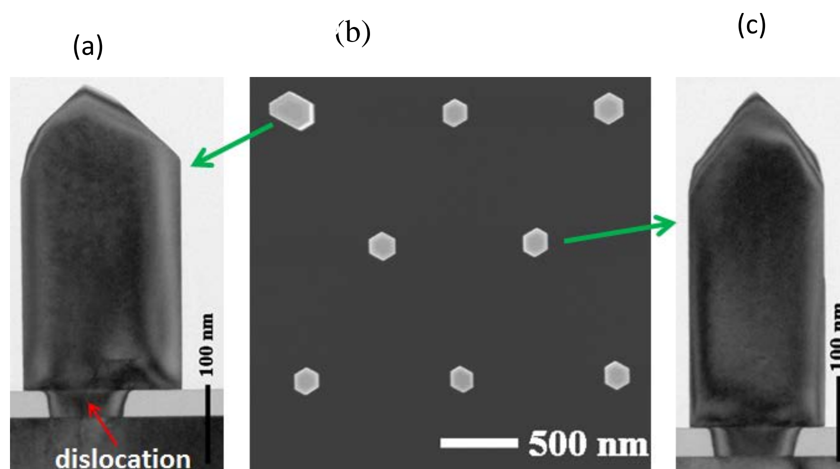

*Figure 10. Identification of GaN NWs with a dislocation propagating from the underlying GaN buffer layer. **a**) A TEM image showing asymmetric growth caused by deflection of a dislocation from underlying GaN buffer layer. **b**) A top view SEM of GaN NWs. **c**) A TEM image of a symmetric GaN NW which is free of dislocations.*

The ability of continuously, selectively grow GaN nanowires to filter out dislocations was investigated. Typically, dislocations in the underlying buffer layer do not extend into the nanowires but when dislocations extend through the mask openings they are seen to deflect towards the side facets at early stages of the growth as shown in figure 10a. The intersection of the bent dislocation to the side facet makes the corresponding side facet grow faster than other facets, rendering the wire shape to be asymmetric, as seen from figure 10a and 10b. Six such asymmetric wires were selected for characterization by TEM and dislocations were confirmed in all of them. GaN NWs without dislocations have symmetric hexagonal shape as shown in figure 10b and 10c. In our NW growth with continuous flows, the formation of asymmetric wires is controllable.

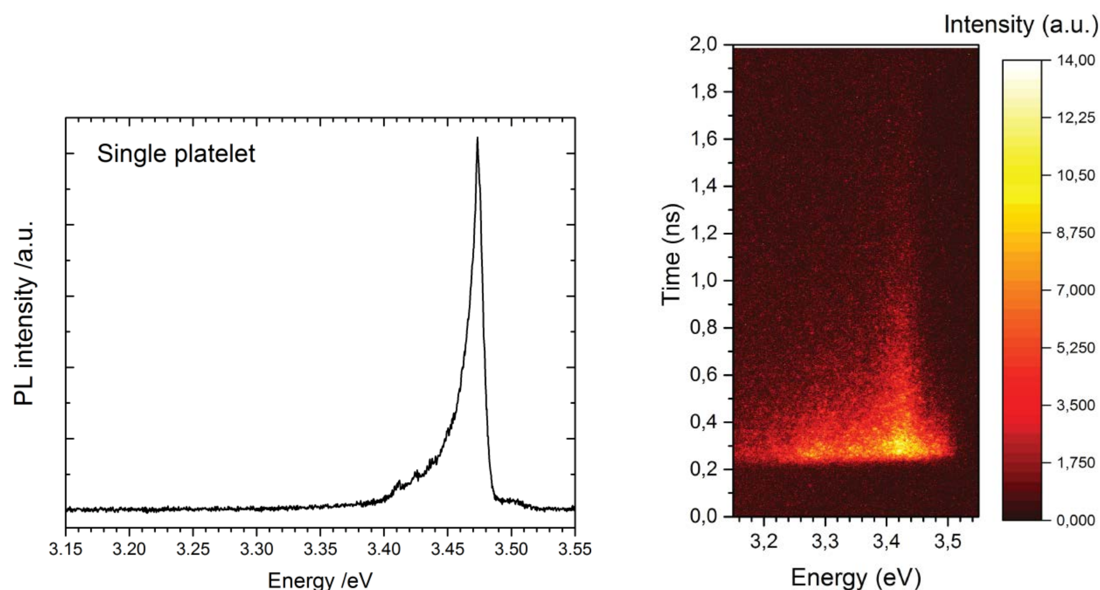

Figure 11. Left: PL spectrum at 8 K from a single GaN platelet which was transferred to a substrate of Au/Si. Right: Decay of donor-bound exciton at 4K from a single GaN platelet which was transferred onto an Au/Si substrate. The lifetime is 400 ps.

Uniform wafer-scale arrays of GaN platelets were developed by growing a GaN shell on the dislocation-free GaN NWs mentioned above. $\{10\bar{1}1\}$ planes are firstly formed at the wire top when the shell growth starts. Because of the extremely low growth rate, $\{10\bar{1}1\}$ planes force the GaN to grow downwards with the $\{10\bar{1}1\}$ planes maintained, as shown in figure 12a. With this pyramidal growth fashion, no c-plane is formed. However, we will show how the *c-plane* can be obtained through controlled change of the epitaxial growth mode, which leads to the formation of GaN platelets as shown in figure 12b and 12c. The size of the *c-plane* can be

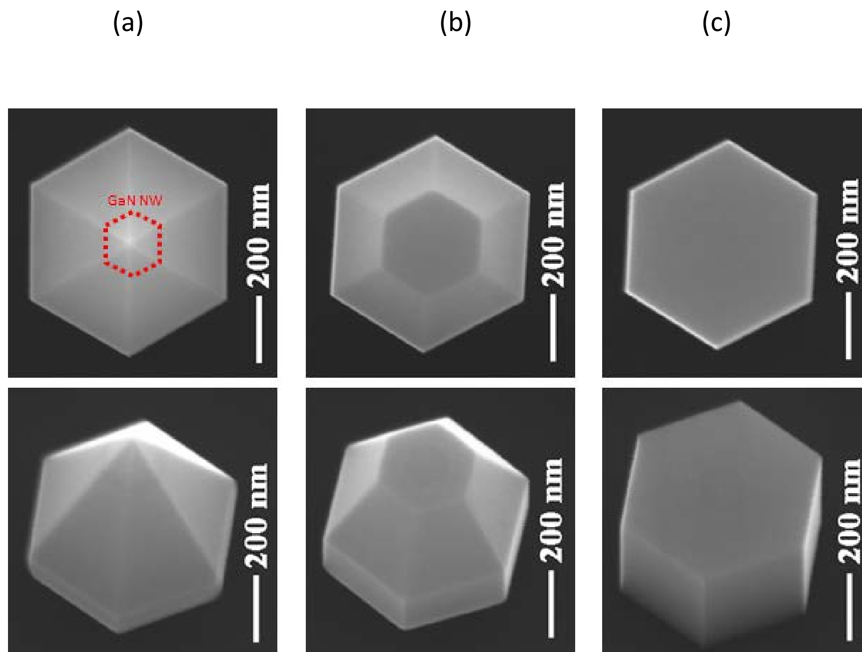

Figure 12. Top-view (top row) and tilted-view (bottom row) SEM images of GaN shell growth on GaN NWs. ***a****) Pyramidal shell growth without c-plane. Dotted lines show the profile of GaN NW.* ***b****) &* ***c****) show controlled platelet growth with varied c-plane size.*

increased by totally eliminating the $\{10\bar{1}1\}$ planes (figure 12c). Time-resolved photoluminescence was measured on a single GaN platelet which was transferred onto an Au/Si substrate. It shows the emission of donor-bound excitons and the lifetime is 400 ps (figure 11).
The method of pyramidal growth and subsequent flattening of the pyramids was extended to the GaInN materials system with the ambition to synthesize materials for defect-free GaInN red and yellow emitting NW-LEDs. A composition of 11% In was found in the platelets (Fig. 13).

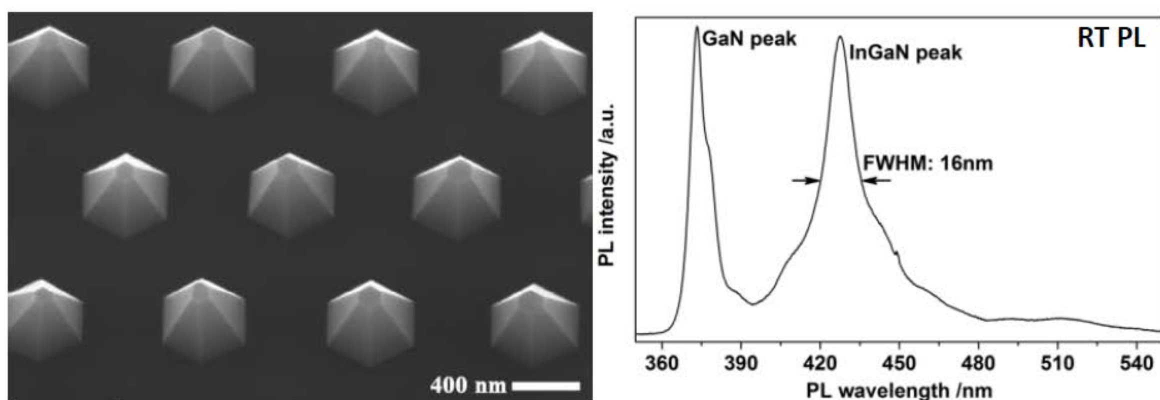

Figure 13. Left: SEM image of InGaN pyramids grown selectively in holes opened up in a SiN growth mask. Right: PL spectrum obtained from the material upon optical excitation.

By inserting a GaInN quantum well on the c-plane we show that the wavelength of the emission can be tuned by growth parameters (Fig. 14).

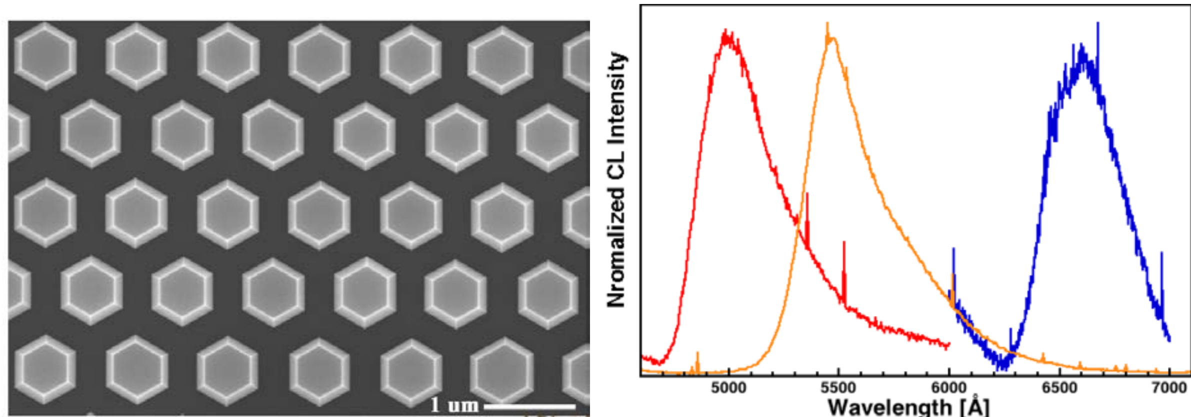

Figure 14. Left: SEM image of the GaInN platelets with embedded GaInN quantum wells for emission. Right: spectrally resolved CL from the platelets.

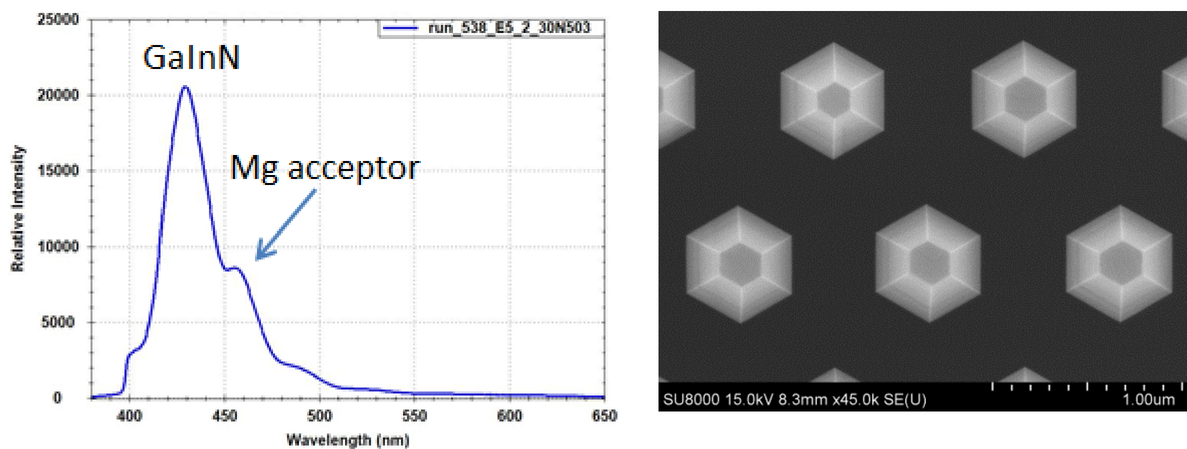

Figure 15. Left: a PL spectrum at room temperature on Mg-doped GaInN platelets; Right: a full LED structure based on GaInN platelets with p-GaInN at the top of pyramids.

Mg-doping on the GaInN platelets was studied. Because of the narrow band-edge emission from GaInN platelets, the emissions related to the Mg acceptor was found at the lower energy side (figure 15). Such p-GaInN growth was applied to the single QW on the GaInN platelets and a full LED structure was obtained as shown in the right SEM image in figure 6. Compared with the LEDs on c-plane GaN template, our structure offers smaller lattice mismatch between the GaInN template and the QW, which means better material quality and less quantum-confined Stark effect.

Development of III-V radial heterostructure NW materials for light emission.

III-V heterostructure growth has been developed with respect to materials composition and doping in the axial as well as radial geometry in order to produce red light emitting nanowire diodes.

TESn is the preferred n type dopant of SiH_4, DTBSe and TESn with respect to dopant level achieved and control thereover.

Contactless electron off axis electron holography was used to determine shifts in the electrostatic potential, being a way to quantitatively measure doping.

By calibrating electron off axis electron holography in comparison to other methods of evaluating doping, it could be used to quantitatively determine doping level.

We found that doping by use of DEZn affects the materials composition of GaInP NWs where the GaInP materials composition was assessed by XRD, TEM and PL.

Axially homogeneous p doped GaInP NWs were grown by use of a method using in situ ramping of the TMI flow.

Parameters and growth scheme for full radial NWLED in (Al)GaInP were developed and lattice matched core shell NWLEDs were grown and characterized with respect to structural and electro optical materials properties. Phase segregation of Al and Ga during radial growth of shells was observed by use of TEM.

Hall voltage measurements was used to determine the n doping in the V-III nanowires, and doping carrier concentrations of $3x10^{17}$ cm^{-3} in the nanowires with highest S doped NWs were found. Lower doping levels were not possible to evaluate due to electrically non-transparent contacts.

IQE measurements of the NWLEDs with ideality factor about 3 are pending. For more details we refer to D1.6.and to the corresponding LED-section in WP3 below.

WP2. Characterization of NW-LED structures.

Structural characterization of radial GaInP/AlGaInP nanowire quantum well structures by high resolution STEM and STEM-EDX

High resolution STEM and STEM-EDX were applied to radial GaInP/AlGaInP nanowire quantum wells grown by MOCVD to study the sharpness of the heterojunctions and the compositional distribution of materials.

More than five different samples in which the Al precursor, trimethylaluminum (TMAl), was varied systematically were investigated to obtain the right concentration of Al in the AlGaInP layers. Results from one of these samples are summarized in figure 16. In all cases, Al enrichment with In and Ga deficiency was observed at the corners of the AlGaInP layers in the cross-section perpendicular to the nanowire axis. The GaInP/AlGaInP interfaces were relatively sharp.

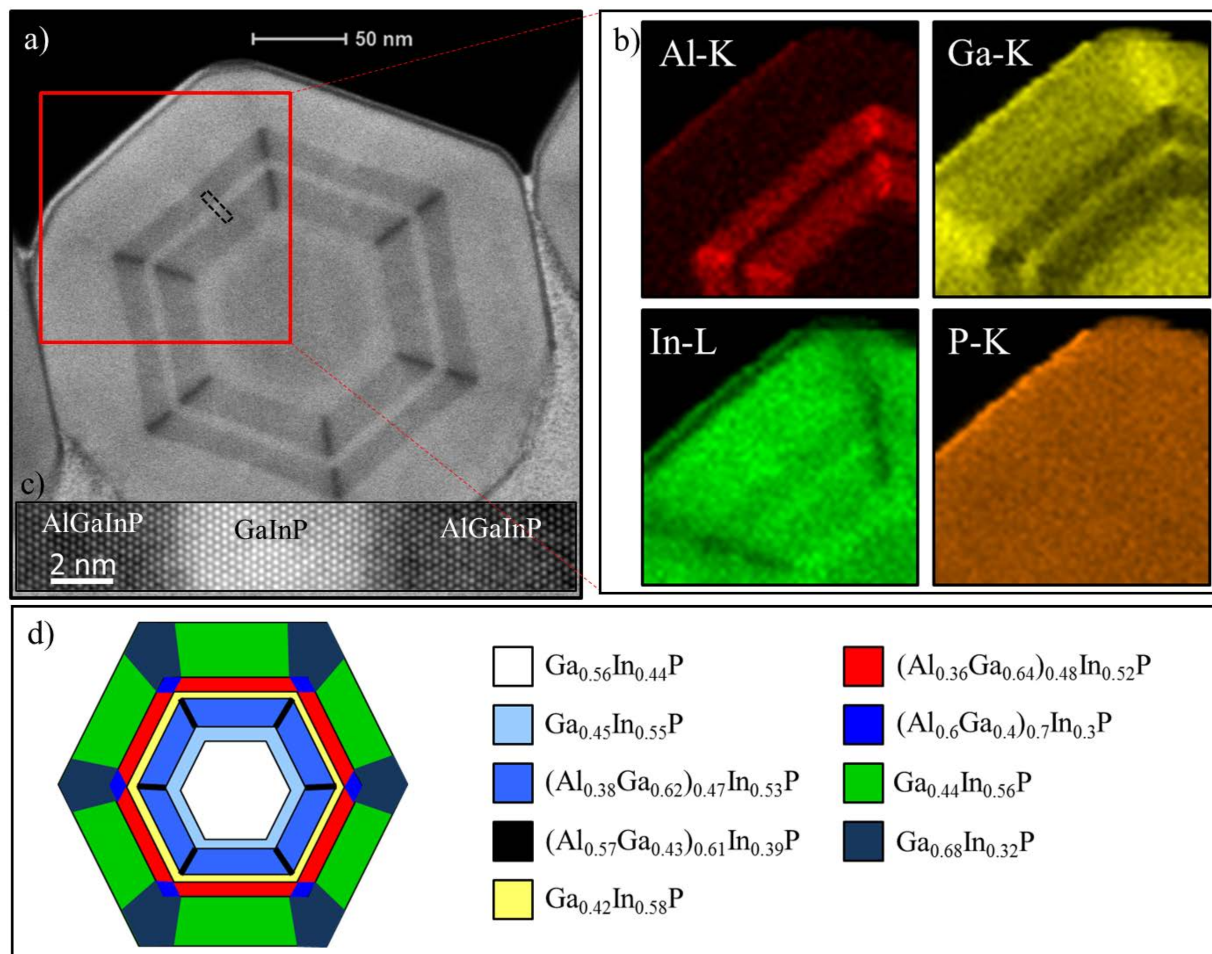

Figure16. An example of compositional and structural characterization of radial GaInP/AlGaInP nanowire quantum well structures by the means of STEM. a) HAADF-STEM image of a FIB-prepared cross-sectional specimen. b) STEM-EDX map from the region marked with the red box in the HAADF image, showing the Al, Ga, In and P distribution. c) Atomic resolution STEM image from the AlGaInP/GaInP interface, the region marked with the small black box in the HAADF image. d) Material composition of different regions of nanowire, calculated from the EDX measurements.

Structural characterizations of NWs using X-rays: Single GaInN/GaN nanowire characterization

We present detailed nanoscale strain mapping performed on a single, 400 nm thick and 2 µm long core-shell GaInN/GaN nanowire with an x-ray beam focused down to 100 nm. A scanning electron microscopy (SEM) image of the typical NW from the same sample is shown in figure 17(b). The sample was carefully cleaved leaving the single isolated nanowire at the tip of the 60° corner of the substrate, as shown in figure 17(a). Strain mapping was performed at the X-ray nano-beam end-station [1] of the P06 beamline at the Petra III synchrotron radiation facility (Germany).

Figure 17 (a) Experimental set-up used for SXDM. A single NW at the corner of the sample was positioned in the focus of the x-ray beam and scanned in the xz plane at different angles. (b) SEM image of the NW. The white ellipse represents the FWHM of the incident beam (100x 150nm).

The strain maps were calculated from the peak positions for three different areas of the NW. From the strain maps corresponding to the GaN core (see figure 18 a) we notice sharp strain gradients at the bottom of the NW, showing an apparent difference of the lattice constants in the NW and the underlying substrate Larger in-plane strain ε_{xx} is observed along the sides of the core, especially near the tip. Both strain components in the core are asymmetric with respect to the left and right sides of the NW. The tensile strain is larger in the left side of the core. This distribution may be caused by an asymmetric relaxation of the GaInN shell, as will be discussed next.

From the intensity map of the region B, shown in figure 18(b), we can see that it originates mostly from the narrow stripe on the left of the NW, which corresponds to the left side of the GaInN shell. The intensity is twice as strong at the top, compared to the bottom (see figure 18(b)), which is in agreement with an uneven distribution of the thickness of the shell, as measured with the cross-sectional SEM. From the strain maps in figure 18(b) we can see that the left side of the shell is compressed in the z direction in order to become coherent with the core.

The intensity and strain maps obtained for the region C, containing the diffuse signal, are shown in figure 18(c). From the intensity map it can be seen that it originates mostly from the top-right part of the GaInN shell. From the SEM image in figure 17(b) we can see that the surface of the GaInN shell is especially rough at the upper part of the NW. This explains the highly diffuse signal in the region C in reciprocal space. From the strain maps we can see that the in-plane and out-of-plane strain components have similar values, which corresponds to the relaxed $In_xGa_{1-x}N$ with $x_{In} = 0.32$.

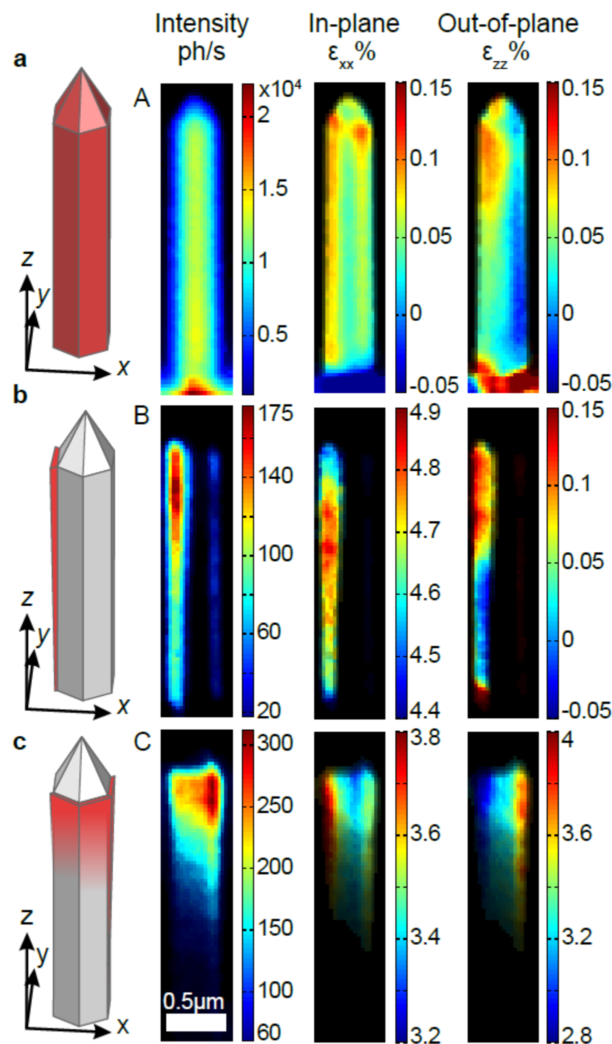

Figure 18. Intensity and strain maps of three different NW regions. The sketches in the left column show the regions of the NW that contribute to the corresponding maps. From the intensity map of region B we can see that it mostly contributes to one side of the shell. Region C, corresponds to the relaxed part of the GaInN shell on the right and top parts of the NW.

NW-based light emitting diodes comprise a macroscopic die with thousands of identical nanowires, each one acting as an independent light emitter. Using the single NW characterization one has to demonstrate that the single NW chosen to be measured was not a statistical outlier, but can represent an entire ensemble. Reciprocal space mapping (RSM) was performed on ensemble of nanowires at beamline I811 at Max Laboratories in Sweden, giving the average strain state in the large number of nanowires. RSMs of the (10-11) peak measured for the ensemble are compared to the single NW measurements done with the nano-focused beam in figure 19(a) and (b), respectively. In both cases we identify a signal from both the relaxed and the strained GaInN shell. This similarity allows us to extrapolate the findings based on the single nanowire to the entire sample, although in general this is not the case.

In conclusion, we have demonstrated how the combination of a nanofocused x-ray beam and SXDM can be used to map the strain distribution in a single NW with a resolution of about 100 nm. We have found that the strain distribution in the GaN core caused by the lattice mismatch at the GaN/GaInN interface is inhomogeneous. Asymmetry in the axial strain relaxation is present, with one side of the shell being fully pseudomorphic with the core and the other side plastically relaxed. In this we also demonstrate fully strained 15-28 nm thick $In_{0.32}Ga_{0.68}N$ shells on GaN NWs. This exceeds the predicted critical thickness in the planar

structures, which does not exceed 10 nm, demonstrating the advantages of the nanowires. However, uneven strain relaxation can lead to inhomogeneous material incorporation which has impact on the device performance. We have demonstrated here that strain mapping with the nano-focused x-ray beam has proven to be an excellent tool for measuring such nanostructures, which are too thick for alternative characterization methods.

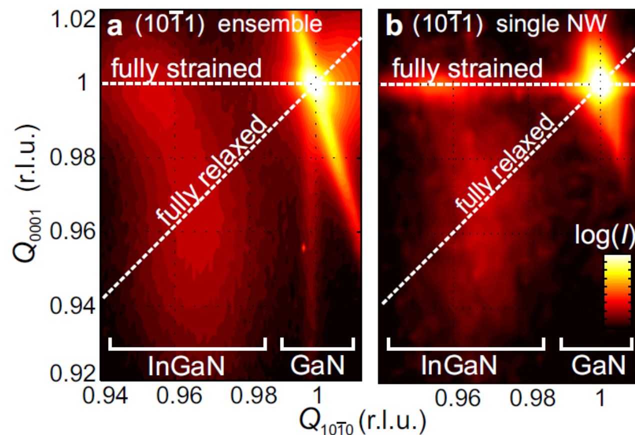

Figure 19. Reciprocal space maps of the (1011) peak measured for an ensemble of NWs (a) and the single NW (b). Both RSMs show similar features, indicating that the single NW is representative for the whole ensemble.

These results are from a simpler test sample compared to a real NW-LED structure. It does however demonstrate the power of these nano-RXD measurements to discover strain inhomogeneities in NW objects. In the future there is hope that such measurements can be extended to map the strain state of the MQW active region in a NW-LED.

Improving the spatial resolution in photoluminescence from wires by using SILs

The spacing of the wires in typical arrays for LED devices is about 1µm. This is on the border of what can be resolved in our micro-PL setup. In order to improve this we are currently experimenting with various designs of solid immersion lenses (SILs). These are truncated spheres that we have fabricated ourselves as they are not commercially available. We have some preliminary results on this study. The simplest test is to study well-defined patterns and to compare with and without the SIL. This is presented in figure 20, using an array of wires with a 400nm-spacing. The left image is the image without the SIL and the right image is with the SIL. It is clear that the optical resolution is improved where the individual wires are accessible with the SIL.

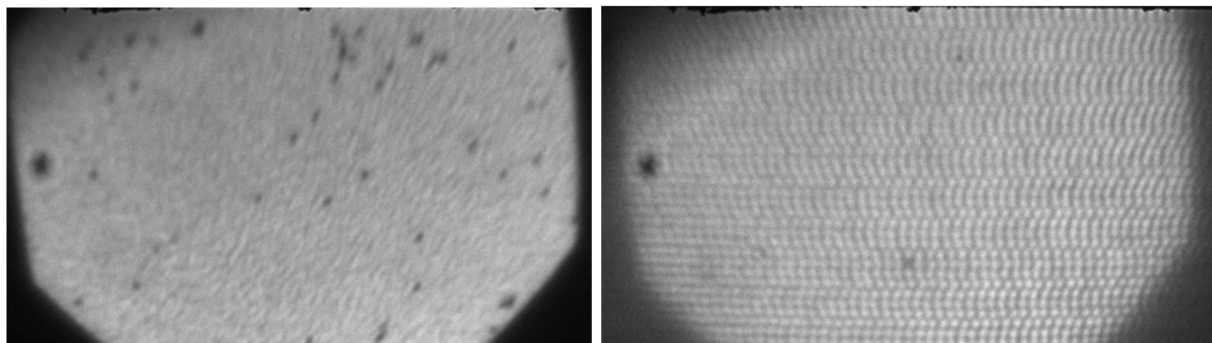

*Figure 20. Two white ligth images of an array of wires with a 400nm pitch. Without the SIL (**left**) the image is grainy and shows no periodicity. With the SIL (**right**) there is a clear periodicity of white spots. The improvement in resolution is obvious.*

In PL imaging, we have not yet got the setup working properly. The laser needs to be spread over a larger area. Figure 21, shows some examples of PL imaging of wire arrays. The first example is InP with a 400nm pitch. Without the SIL, there is no hint of resolving the individual wires. All that is visible is the emission under the laser spot. With the SIL, there is a pattern of bright spots of the individual wires. The SIL is also used on GaInN pyramids with a pitch of 1µm. In this case, the bright spots are better resolved, as expected due to the larger pitch.

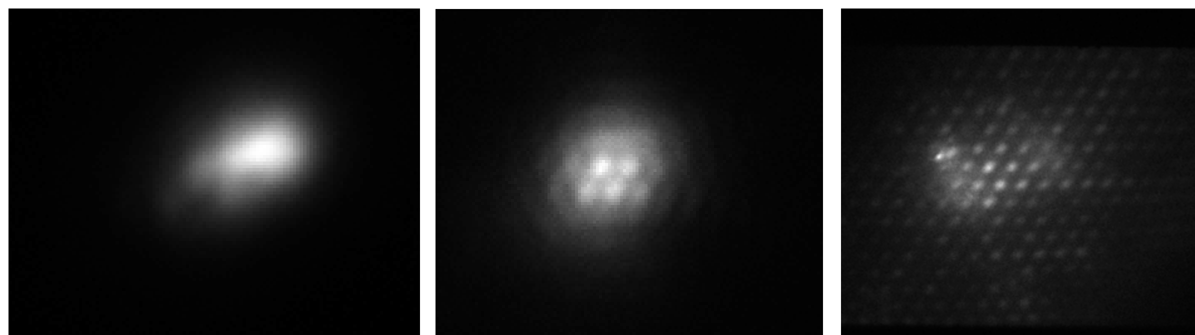

*Figure 21. **Left**: The emission from an array of InP wires with a pitch of 400nm. In this image without the SIL, there is no structure in the bright spot excited by the laser. **Centre**: When the same array is imaged with the SIL, bright spots corresponding to the individual wires can be observed. **Right**: As the pitch is increased to 1µm, the improvement is even more pronounced, here the arrays consisted of GaInN pyramids.*

WP3. NW-LED devices in the project.

Green III-nitride core-shell nanowire LEDs have been demonstrated by Glo with peak EQEs exceeding 35% and EQEs at 20 A/cm^2 equivalent to the performance of commercially available planar devices. The performance characteristics of the green NW LEDs are consistent with IQE ~ 40%. The devices exhibit good p-type layer conductivity and low defect density.

Figure 22 shows the EQE of green NW-LEDs as of M18 of the project and M24 of the project, plotted against current. This plot illustrates that through optimization of the epitaxial growth process to increase the volume of green-emitting QW material on the sidewalls of the nanowire, the efficiency at high current densities can be substantially increased. In these two efficiency versus current curves, the volume of the QW is increased by a factor of more than two. This was accomplished by increasing the molar flux of TMIn and TEGa in the epitaxy reactor during the deposition of the QW. Another element of increasing the volume of QW material is increasing the density of nanowires formed on the GaN template. In the device shown for M18, the nanowire spacing (or pitch) is 1 µm, whereas for the device shown for M24, the nanowire spacing is 0.7 µm. The nanowires are formed in a hexagonal pattern, therefore this reduction in spacing corresponds to double the number of nanowires per unit area of substrate in the M24 case. Figure 23 shows an optical microscope image of a portion of the LED active area for the M18 device, while the NW-LEDs are operating. Full-wafer nanoimprint technology is capable of forming even denser arrays of holes in the selective area growth mask used to create the nanowires.

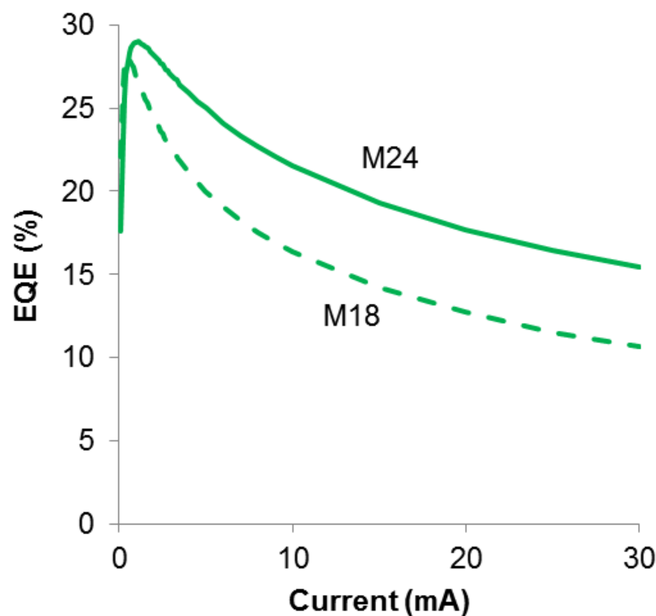

Figure 22. External quantum efficiency (EQE) of green nanowire LEDs as of month 18 (M18) and month 24 (M24) of the project. The EQE is shown for LEDs packaged into dome lenses on Ag-coated TO-5 headers with an n=1.52 silicone dome lens.

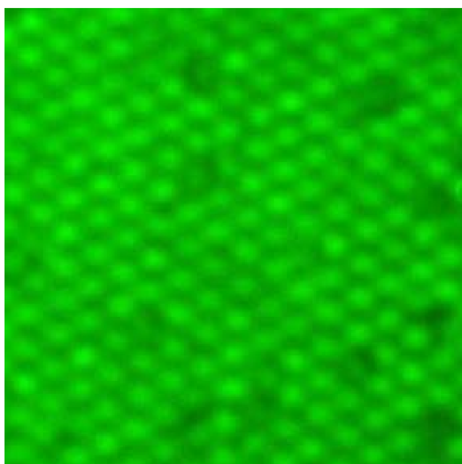

Figure 23. Optical microscope image of a portion of the M18 NW-LED while the device is operating. The bright spots are nanowires while the dark region between the bright spots is the open area on the GaN template. The nanowire pitch is 1 µm

By further reducing the nanowire pitch to e.g. 0.5 µm, the EQE of the green NW LEDs will be further improved. Our estimation is that at 0.5 µm, which corresponds to a 2x increase in number of nanowires per unit substrate area over the M24 case, the EQE at 20 A/cm^2 will be improved to 22% or higher.

Processing technology for green NW LEDs has also been advanced from M18 to M24. In both cases, the LED has a anode contact (Al/Ti/Au) deposited on the n-type GaN "buffer layer" which is located underneath the selective area growth mask. The buffer layer is grown on sapphire in the cases of these LEDs, although Si has also been used. The cathode contact is a transparent conducting oxide (TCO) deposited across the surfaces of the nanowires, which are p-type. An Al/Ti/Au wire-bonding pad is deposited on the TCO to complete the cathode contact. In the M24 device, the TCO is recessed from the edges of the array of nanowires, whereas in the M18 device the TCO reaches the edge of the nanowire array. The M24 devices

suffer from less resistive shunt leakage compared to the M18 devices due to this change, and thus have an increased EQE especially at low currents.

The green NW LEDs have forward voltages (V_fs) of approximately 3.2 V at 10 A/cm^2 forward drive current. The V_f responds to traditional parameters for planar GaN LEDs, such as temperature for "activation" of Mg dopant atoms in the p-type GaN layer, and Mg doping concentration in the p-type GaN layer. At M18, the V_f was approximately 3.6 V and by optimizing the dopant levels and activation process parameters (such as time and temperature) the voltage was reduced by 0.4 V by M24.

NW-LED wafer process.

GLOINC demonstrated that it is possible to produce nanowire LEDs using a flip-chip process technology, thereby enabling the integration of these LEDs into systems with large numbers of devices where the otherwise-needed wire bonds are prohibitively expensive or result in yield or reliability problems of the integrated system. It is well known in the LED field that flip-chip devices require highly reflective p-type spreading contacts, in order to exhibit high optical extraction efficiency. The commonly used metals are Al and Ag. GLOINC evaluated both of these metals. Figure 24 is a cross section schematic of a flip-chip nanowire LED affixed to a submount.

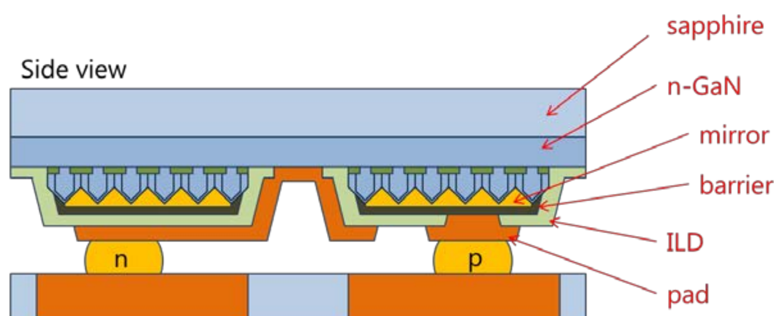

Figure 24. Cross-section sketch of a flip-chip nanowire LED

It is also a fundamental necessity of a flip-chip device that the anode and cathode contacts be formed of solderable metal. Most commonly used is AuSn. Due to the solid-phase reactions of these various metals and the potential impact thereof on device reliability, so-called barrier metals are typically provided between the reflective contact and the solder metal. A key requirement of any metal film in a flip-chip device is that the metal film is substantially free of voids. While this is typically straightforward to achieve on planar films, the high-aspect ratio topology of the nanowire LEDs tends to produce textured films (the adjective textured refers to both the commonly known morphological definition, and the term of art used by crystallographers).

Figure 25 is a cross-section SEM taken of a nanowire array with a layer of TiN sputtered on the array (the top-most film); this is considered an unacceptable barrier metal surface morphology

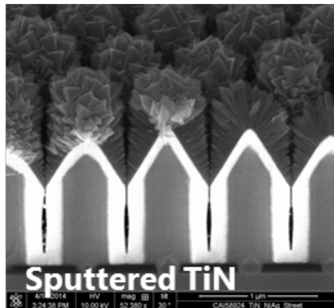

Figure 25. Cross section SEM of nanowire array (gray and white obelisk shapes) with a sputtered layer of TiN deposited on top.

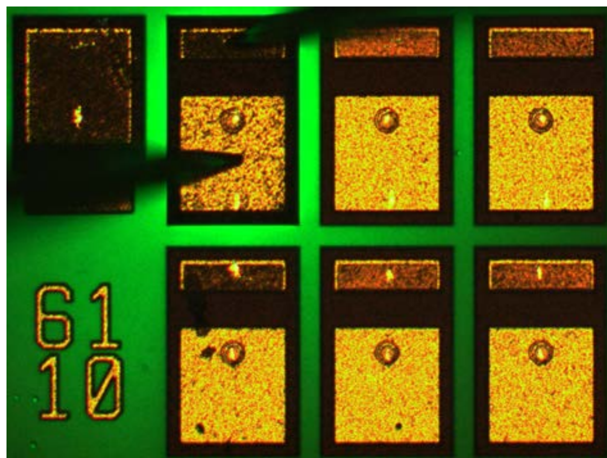

Figure 26. Plan view optical microscope image of a nanowire flip-chip LED with forward bias applied. Light from the active region (underneath the metal contacts) is seen scattering off of the substrate back side.

GLOINC selected e-beam deposited Mo as the preferred barrier metal. Additional deposition of Au solderable contacts was performed. Figure 26 is a plan-view optical microscope image of a flip-chip nanowire LED with power applied. Light from the active region, scattered off of the substrate back side, is seen surrounding the metal contacts. GLOINC has not characterized the optical extraction efficiency of this device configuration. Depending upon the results of those data, additional work on contact reflectivity may be required to realize a commercially competitive device.

Manufacturability and cost assessment

GLOINC presently estimates the manufacturing cost of GaN/InGaN nanowire LEDs to be approximately 20% higher than the manufacturing cost of GaN/InGaN planar LEDs, and anticipates that this cost differential will decrease over time as knowledge is accumulated and engineering development is done to specifically address some sources of cost increment.

The manufacturing process for a GaN/InGaN nanowire LED is, at a high level, identical to the manufacturing process for a GaN/InGaN planar LED, with two major exceptions, both of which are associated with the epitaxial growth process. The first exception is that the epitaxial growth process is done in two steps through the MOCVD reactor, as opposed to one step. In the nanowire LED process, the first MOCVD growth step is performed in order to create a GaN template layer on a substrate such as Al_2O_3 or Si. Then, nanoimprint lithography is used to create a selective area growth mask on the template. Finally, the wafer is loaded into the MOCVD reactor and the nanowire LED array is grown.

One source of additional manufacturing cost is associated with a longer cycle time in the MOCVD reactor, which adds depreciation cost. GLOINCs current estimate for MOCVD cycle time increase is 10%. The growth of the GaN template layer is more rapid than the growth of the GaN template used for GaN/InGaN planar LEDs, since the dislocation density of this film may be much larger for the selective area growth nanowire LED device structure. Growth of the nanowire LED array is similar in cycle time to the growth of the active layer and p-layer stacks used in planar GaN/InGaN LEDs. Because large multi-wafer production MOCVD reactors have large thermal masses, cool-down and heat-up times are typically 45 minutes to one hour long. Because two complete MOCVD cycles are required, there are four heat-up/cool-down cycles per GaN/InGaN nanowire LED wafer, as opposed to one heat-up/cool-down cycle per GaN/InGaN planar LED wafer. The net result is that the MOCVD cycle time is somewhat longer for GaN/InGaN planar LEDs.

A second source of additional manufacturing cost is the additional manufacturing steps of depositing the dielectric growth mask, performing nanoimprint lithography on that growth mask, and dry etching the growth mask to form a template for selective area growth of the nanowire array. The cost of these steps individually is relatively low. The dielectric growth mask deposition may be done in simple large scale batch furnaces which can process 100 or more wafers at a single time, for a total throughput around 100 wafers per hour. The throughput of the nanoimprint lithography step is on the order of 50 wafers per hour, depending upon the details of whether thermoplastic or UV imprint is used. The dry etch step to form the holes in the selective area growth mask may be performed on multi-wafer ICP-RIE etchers, with a throughput on the order of 50 wafers per hour. The throughput of the MOCVD step is about 5 wafers per hour, much lower than the growth mask process step.

During the early stage of ramping the volume of the GaN/InGaN nanowire LED manufacturing process, it is anticipated that the cumulative yield of the manufacturing process will be somewhat lower than is achieved today in state-of-the-art manufacturing facilities for planar GaN/InGaN LEDs. Most of this additional yield fall-out can be attributed to the selective area growth masking process, and possibly some decrease in within-wafer LED yield or across-wafer non-uniformity. Additional process control points may be implemented to screen non-conforming materials from subsequent process steps, minimizing the cost of yield fall-out. Within-wafer uniformity of GaN/InGaN nanowire LED performance is consistent with the uniformity of state-of-the-art planar GaN/InGaN LEDs today. For example, the within-wafer standard deviation of peak emission wavelength is measured to be 1.5 nm for GLOINC's green GaN/InGaN nanowire LEDs on 50mm substrate, while it is 2.1 nm for planar GaN/InGaN LEDs on 50 mm substrates.

NW-LED performance characterization and reliability study.

GLOINC characterized the performance of a second generation of GaN/InGaN green-emitting nanowire LED in Month 24, and compared to the performance of a first generation demonstrated in Month 18. Figure 22 above shows a comparison of the external quantum efficiency characteristics of these two generations of GaN/InGaN nanowire LEDs. The EQE of the second-generation devices is greater, especially at current densities greater than 3 A/cm^2. This performance improvement was generated in two ways. First, the density of nanowires per unit substrate area was increased by reducing the pitch of the nanowires on the selective area growth mask and GaN template from 1.0 um to 0.7 um (a factor of 2 increase).

Second, work was done on optimizing the growth conditions (principally molar flow rates of Ga and In precursor chemicals into the MOCVD reactor).

In addition to having a higher EQE, the nanowire LEDs demonstrated in Month 24 also had lower forward voltage.

The second generation green-emitting GaN/InGaN nanowire LEDs were subjected to reliability stress tests. The stress condition was 10 A/cm^2 forward current in an ambient temperature of 90ºC. After 2.000 hours of stress, the GaN/InGaN nanowire LEDs exhibited less than 10% decrease in optical output, and negligible change in forward voltage and emission spectrum. Figure 27 shows lumen maintenance data from more than 30 LEDs tested from two wafers, after 2.000 hours of stress.

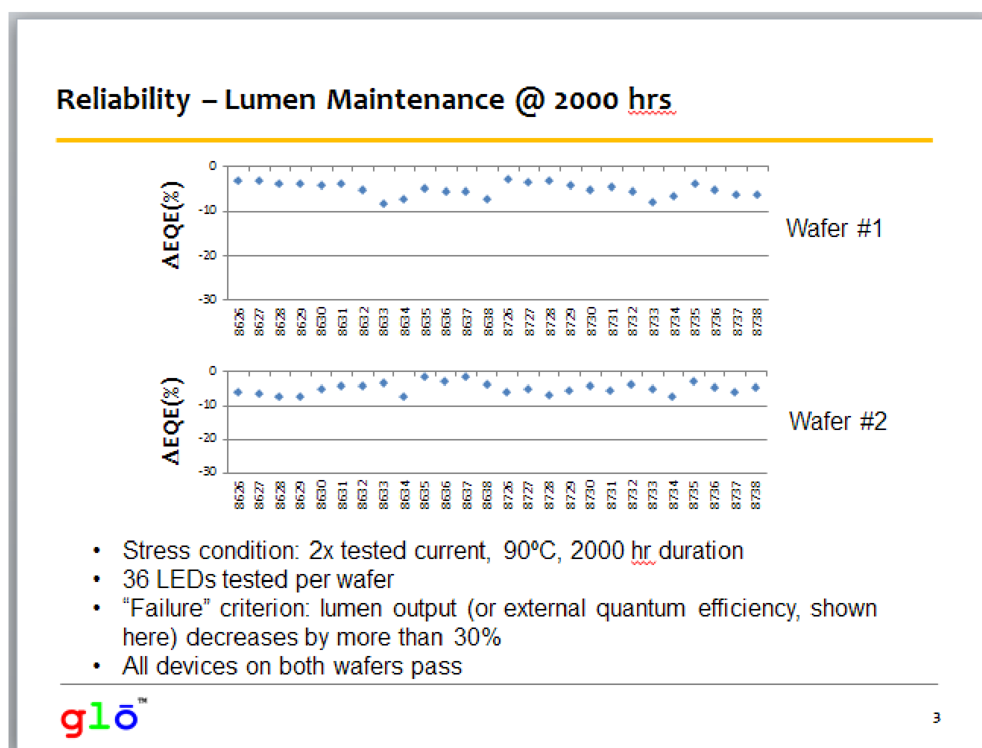

Figure 27. Lumen maintenance data for green-emitting GaN/InGaN nanowire LEDs under high-temperature operating life stress conditions. At 2.000 hours of stress, all devices pass specification.

Optical properties of truncated GaInN nano-pyramids and related LEDs.

An alternative route for the green and even red LEDs is to use GaInN-based structures. In order to avoid the problems related to homogeneity of the ternary core and to circumvent strain-related defects in wires based on a GaN core, we have investigated truncated nano-pyramids of GaInN. Using this approach, we have been able to vary the emission over a large range of emission wavelengths, as illustrated in figure 28. These spectra were recorded from truncated pyramids with different thicknesses of the active layers, but with the same layer compositions. These spectra show that it is possible to tune the emission in the range 500 to

650 nm at low temperatures. Room temperature measurements show that the emission only red-shifts with a small amount. CL imaging further reveals that most of the nano-pyramids are defect free.

The nano-pyramids have also been made into LED devices by putting the active layers in a pn-junction. We recently did some simple tests of one of these structures by contacting a large number of pyramids with nano-probes, (about 25 000). Figure 29 shows a photo of the LED in this study. The green spot is the emission from the pyramids at room temperature.

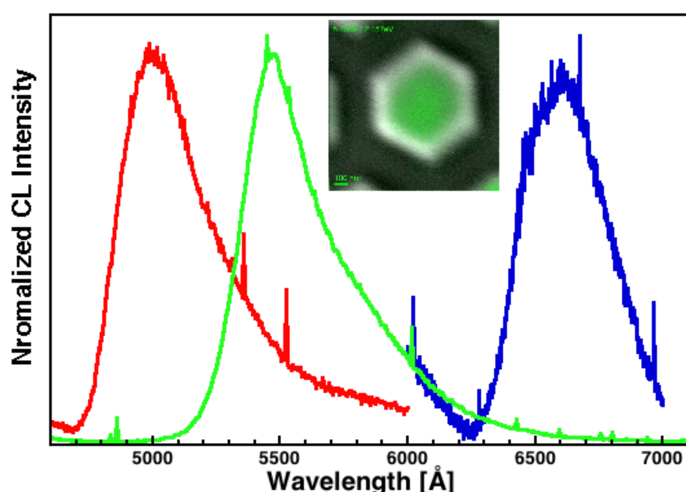

Figure 28. A set of emission spectra recorded from truncated GaInN nano-pyramids. The barriers and active layers have the same compositions for the different samples studied. The only difference is that the active layers have different thicknesses. The spectra were recorded over several pyramids for each sample. The inset shows a colour-composite image of a single pyramid. The grey-scale image is an SEM image and the green is a monochromatic CL image recorded at the peak of the green spectrum. This shows that the emission is very homogeneous from the individual nano-pyramids.

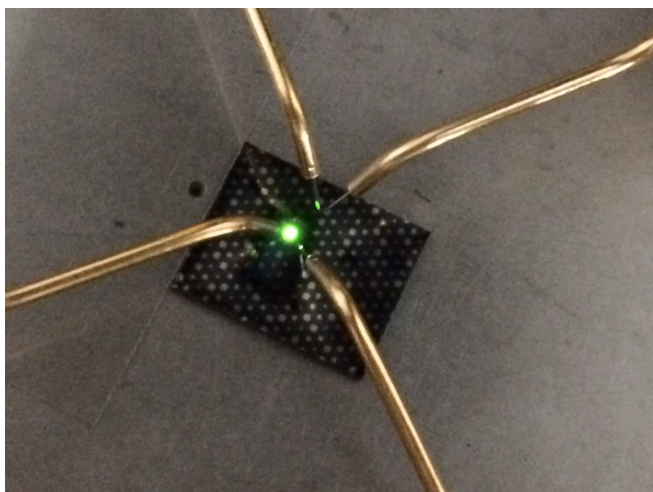

Figure 29. A photo of a simple device based on the nano-pyramid geometry. When a current is passed through the pyramid using nano-probes, the pyramids emits enough light to be detected by a digital camera. The green spot is the light from a large number of NW-LEDs.

III-V nanowire LEDs (AlGaInP material system.)

Recently ULUND has strengthened its effort to demonstrate device performance of our III-V NWLEDs. As briefly mentioned in D1.6 we have modified the epi-structure of the GaInP-

AlGaInP core-shell NWs in order to increase the efficiency. Several modifications were made (Fig. 30):

- The growth time for the upper segment of the p-GaInP NW core was increased to 6 min. The material composition of the ternary p-GaInP NW core was measured to be homogeneous.
- On top of the p-GaInP NW core an n-GaP top segment was added in order to avoid leakage from the outer most shell directly into the core by avoiding the QW.
- The p-GaInP buffer layer (inner most shell) was grown thicker (growth time 2 min instead of 15 s) because the NW core has a smaller diameter than the opening in the SiN_x mask. Thus leakage from the QW directly into the substrate can be avoided.
- The AlGaInP barriers were grown non-intentionally doped instead of p- and n-doped, respectively.
- The bandgap of the AlGaInP barriers were increased up to 150-200 meV in order to force the carriers even more to be trapped in the quantum-well (QW).
- The outer most shell n-GaInP was highly doped with tin (Sn).

The core and shells were grown lattice-matched with compositions of $Ga_{0.47}In_{0.53}P$ and $(Al_xGa_{1-x})_{0.47}In_{0.53}P$, respectively. A series of 3 samples with 3 different i-GaInP QW thicknesses were grown:

- 20 nm (estimated)
- 10 nm (estimated)
- 5 nm (roughly measured by TEM)

Having grown radial GaInP/AlGaInP nanowires, we processed the vertical NW arrays to define the devices and to electrically contact the NWs. Standard UV lithography was used to define 100×100 μm^2 devices on the samples, and the samples were then contacted by sputtering 150 nm of indium-tin-oxide (ITO) on the NWs as a transparent and conductive contact. Electrical measurements on the devices were carried out with a probe station. For all 3 samples bright red emission was observed (Fig 31).For the 3 samples electroluminescence (EL) measurements with an optical detector were performed. We observe the highest peak intensity for a QW thickness of 10 nm. Additionally, we find a slight blue-shift for the thinner QWs (Fig.31.). This could be attributed to quantization in the QW as we decrease the QW thickness.

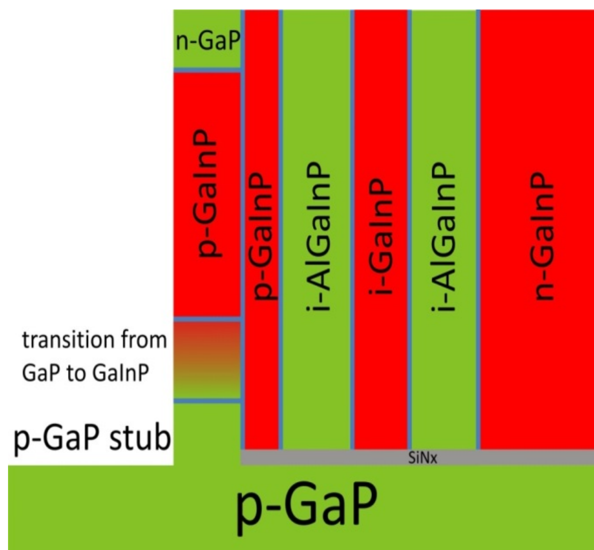

Figure 30. Schematic structure of the radial GaInP-AlGaInP NWs with optimized device design.

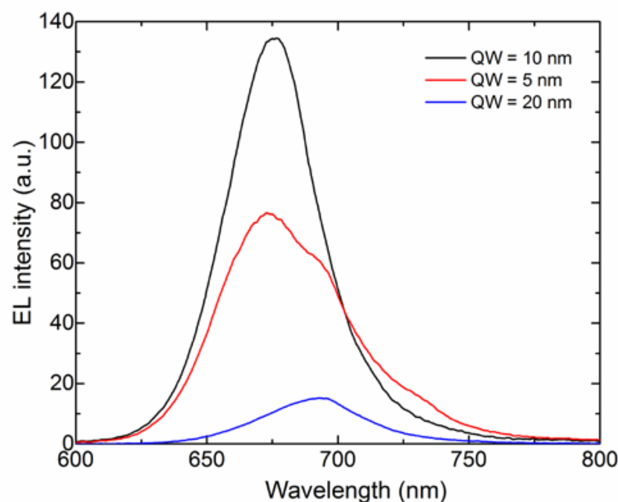

Figure 31. EL spectra of the 3 samples with different QW thicknesses. For all 3 samples the current density was 40 mA/cm^2.

ULUND has not yet measured calibrated IQE/EQE for these samples. We believe that the vertical processing has to be improved by adding a spacer of SiO_2 at the bottom part of the nanowires for impeding any parasitic substrate growth during growth of the shell. We believe that the vertical processing has to be improved by adding a spacer.

For the III-V based NW-LED structures we foresee a similar manufacturing process as for the III-nitride NW-LEDs discussed above. A similar lift-off procedure should also be possible. The cost of the production can also be discussed in a similar way as for the III-nitrides, since a NIL procedure of the substrate is needed prior to growth of the NE-LED structure. At the moment it seems difficult to compete with the present cost of the planar III-V red LEDs.